JOURNAL OF AIRCRAFT
Vol. 45, No. 5, September–October 2008

A New Look at High-Altitude Turbulence

Joshua F. Torgerson* and George Y. Jumper†
Air Force Research Laboratory, Hanscom Air Force Base, Massachusetts 01731

DOI: 10.2514/1.36092

Reconnaissance by aircraft from high altitudes remains an important priority for the Department of Defense. Aircraft at these altitudes experience both traditional mechanical turbulence as well as oscillatory fluctuations of temperature and horizontal and vertical wind speeds, which are attributed to gravity (also called buoyancy) waves. This paper investigates the effects of wavelike behavior on high-flying aircraft, finding high aircraft loads at certain frequencies. Aircraft are most susceptible to problems at the upper range of altitudes. This analysis shows that autopilots based on maintaining a constant Mach number and an indicated airspeed are both susceptible to temperature fluctuations. In addition, temperature changes shift the flight envelope, creating potentially dangerous stall or overspeeding conditions. The absence of temperature variation requirements in current aviation continuous gust load specifications along with a possible deficiency in gust magnitude design requirements at high altitude lead to a recommendation for revisiting high-altitude turbulence requirements and investigating the vulnerabilities of high-altitude unmanned aircraft.

Nomenclature

A	=	gravity wave amplitude, ft
a	=	speed of sound, ft/s
B	=	background stability, 1/ft
$\mathbf{C}$	=	body-inertial direction cosine matrix
C_L	=	coefficient of lift
F	=	thrust, lb
g	=	acceleration of gravity, ft/s^2
I_{yy}	=	aircraft moment of inertia, slug · ft^2
K	=	gust alleviation factor
k	=	horizontal gravity wave number, 1/ft
L	=	aircraft lift, lb
M	=	Mach number
m	=	vertical gravity wave number, 1/ft
$m_{A/C}$	=	aircraft mass, slug
N	=	Brunt–Väisälä frequency. 1/s
n	=	load factor
p	=	pressure, psi
S	=	wing area, ft^2
T	=	air temperature, R
U	=	aircraft-relative horizontal speed, ft/s
V	=	aircraft velocity, ft/s
W	=	aircraft-relative vertical speed, ft/s
w	=	aircraft weight, lb
X	=	aircraft horizontal position, ft
Z	=	aircraft vertical position, ft
α	=	angle of attack
$\delta(X, Z)$	=	vertical displacement of a streamline from its undisturbed height, ft
Θ	=	potential temperature, R
θ	=	aircraft pitch angle
ρ	=	density, slug/ft^3

Subscripts

a	=	air-relative velocity components
f	=	background wind quantity
sl	=	sea level
w	=	wind velocity components

Received 7 December 2007; revision received 6 May 2008; accepted for publication 10 May 2008.

*Aerospace Engineer, Battlespace Environment Division.
†Program Manager, Battlespace Environment Division. Associate Fellow AIAA.

Introduction

DISCUSSIONS with U-2 pilots have led to the realization that aircraft flying above commercial cruise altitudes frequently encounter a type of turbulence that is different from traditional occurrences. The ER-2, which is a civilian version of the U-2S, has flight recorder data openly available at its web site‡, which has good examples of high-altitude turbulence (HAT).

Pilots describe two types of turbulence: mechanical and Mach surf. The motion resulting from mechanical turbulence is described as random bumping in all directions, which is traditional turbulence. The motion resulting from Mach surf, on the other hand, is described as lower-frequency periodic changes in speed over time at more or less the same spatial frequency, often starting at a low but increasing amplitude. The pilots have a temperature display visible in the cockpit and, during encounters of Mach surf, they always notice modest oscillatory changes in the temperature. Their explanation of the Mach surf phenomenon is that these temperature changes alter the speed of sound and, hence, the Mach number of the aircraft. Because the autopilot is designed to maintain a constant Mach number, the resulting speed changes from the autopilot elevator commands create the sensation of surfing the waves of temperature fluctuations. Pilots report that the disturbances often grow to such high amplitudes that the autopilot either automatically disengages or the pilots themselves must take manual control to avoid a dangerous situation.

As described by Ehernberger [1], the problem of high-altitude turbulence has been known since U-2 aircraft began flying in the early 1950s. Although turbulence is less frequent at high altitudes, it can be severe. It occurs most frequently in the winter and is often detected over mountains. As noted by Ehernberger, there is such a scarcity of high-altitude data that experts have been relying on atmospheric models to explain the phenomenon. The modeling activity has continued with ever-increasing resolution since that paper.

High-altitude turbulence that is not directly associated with close proximity to a jet stream is generated by gravity waves. For an extensive review of high-altitude gravity waves and wave breakdown, see Fritts and Alexander [2]. Flow over mountains, storms, and jet streams can create local turbulence and, when this disturbed air is forced to deviate in a direction with a vertical

‡Data available online at http://www.nasa.gov/centers/dryden/research/AirSci/ER-2/ [retrieved 1 July 2008].

component in a stable background field, gravity (or buoyancy) waves are created. As the waves propagate upward into lower-density air, their amplitude increases in magnitude. The waves induce periodic variations in horizontal and vertical wind velocity and temperature. Waves can reach critical levels at which they reflect or break into turbulence, or when conditions are right they can simply grow in magnitude to the point at which they become unstable. Both the Mach surf and mechanical types of turbulence experienced by U-2 pilots can be explained by the various stages of HAT evolution (waves and breakdown). Horizontal wavelengths on the order of $\frac{1}{2}$–1 mile, which appear to be close to autopilot resonant modes, are of a shorter wavelength than those normally associated with gravity waves, yet longer than lengths usually associated with atmospheric turbulence. It is possible that these lengths correspond to intermediate structures related to the breakdown of gravity waves into turbulence [3].

Design requirements for aircraft turbulence are contained in the Federal Aviation Regulations, Part 25, Section 341, and Appendix G [4] for civilian aircraft and the Joint Service Specification Guide (JSSG-2006) [5] on aircraft structures for military aircraft. These documents include discrete and continuous specifications for horizontal and vertical gusts, where discrete is modeled as a single gust and continuous as a power spectral density (PSD). Variations in temperature are not included, yet they have an important effect on the systems as will be shown in this paper.

The U-2 has been operating successfully since 1955; a description of its mission, features, and background is provided by the Air Force fact sheet.[§] The aircraft is able to mitigate HAT because pilots typically take manual control at its first sign. All high-flying aircraft such as the U-2 fly with a constrained envelope. These aircraft have a narrow band of viable flight speeds between stall and overspeeding, making the pilot's job of maintaining controlled flight difficult during a turbulent encounter. The capability of pilotless aircraft, such as the Global Hawk, to sense and properly react to HAT is largely unknown.

With the great progress that has been made in the modeling of high-altitude mountain and other waves, it seem to be an opportune time to simulate flight through these predictions of the waves and their breakdown into turbulence in the literature. The objective of the study presented here is to determine through simulation the impact of high-altitude turbulence on high-altitude aircraft, to compare the simulations to flight experience, and to investigate methods to mitigate the effects of these waves on the aircraft. Specifically, this paper addresses 1) the mathematical models used for the simulation including the aircraft and autopilot and the response of the system to traditional gust sensitivity, a simple mountain wave model, and the results of a gravity wave breakdown simulation; 2) an investigation of the effect of changes in air temperature, as experienced in a gravity wave field, on an autopilot; and 3) the effect of temperature changes on the flight envelope.

Simulation

The impact of atmospheric turbulence on an aircraft is a function of both the atmospheric condition and the aircraft design. Simulation is a way to investigate the interaction between HAT and an aircraft. Although U-2 pilots attribute Mach surf to temperature fluctuations disturbing the aircraft's Mach-following autopilot, gravity waves actually create a complicated combination of horizontal and vertical wind speed variations and temperature changes that affect the Mach number. It was decided to develop a 3 degrees of freedom model (altitude, range, and pitch) to investigate the Mach surf phenomenon, because normally no lateral motion is involved in the encounters. The simulation elements included were the aircraft dynamics, aircraft autopilot, atmospheric model, and turbulence model. The Grob G520T Egrett was the aircraft chosen as the basis for the simulation model because of its flight characteristics and the availability of its flight data. The Egrett is a moderately high-altitude research aircraft with a high-aspect-ratio wing. It cruises at 320 ft/s at an altitude of 35,000 ft, but can reach altitudes up to 50,000 ft. It has been fitted with very high-resolution flight instrumentation and has been used extensively to investigate turbulence in the upper atmosphere [6].[¶]

Table 1 Stability derivatives of Egrett aircraft used for HAT simulation

Lift	Value	Drag	Value	Moment	Value
C_{D_0}	0.0078	C_{L_0}	0.52	C_{M_0}	−0.37
C_{D_α}	0.0630	C_{L_α}	5.98	C_{M_α}	−4.87
C_{D_M}	0.0037	C_{L_M}	0.16	C_{M_M}	−0.16
$C_{D_{\delta_e}}$	0.0044	$C_{L_{\delta_e}}$	0.46	$C_{M_{\delta_e}}$	−2.83
——	——	$C_{L_{\dot\alpha}}$	0.39	$C_{M_{\dot\alpha}}$	−0.78
——	——	$C_{L_{\dot\theta}}$	0.10	$C_{M_{\dot\theta}}$	−0.42

The simulation developed used standard flat-Earth equations of motion to model the aircraft and the stability derivative approach for force and moment modeling. Because the simulation was used to analyze flight through various measured and modeled atmospheres, it was decided to use a rectangular coordinate system. Two main reference frames were used: inertial (Earth-fixed) for horizontal position X and altitude Z, and body (aircraft-fixed) for forward and vertical velocities U and W. This allowed typical specification of the wind velocity relative to the ground and accelerations relative to the aircraft body. The orientation convention is such that X and U are forward, Z and W are down, and θ is positive nose up. The inputs to the simulation were aircraft thrust F and elevator angle δ_e, and the outputs were the aircraft state including position, velocity, pitch angle θ, and pitch angle rate. The simulation formulation is identical to the one developed for a previous AIAA conference paper [7].

The following equations define the aircraft motion in the 3 degrees of freedom [8]. First, introduce a direction cosine matrix that transforms vectors in the body frame into the inertial frame:

$$\mathbf{C} = \begin{bmatrix} \cos\theta & \sin\theta \\ -\sin\theta & \cos\theta \end{bmatrix} \tag{1}$$

The body accelerations for an aircraft with mass $m_{A/C}$ and moment of inertia I_{yy} flying at angle of attack α with lift, drag, and moment L, D, and M can be found from Newton's second law and placed in a standard form (where g is the acceleration due to gravity) [9]:

$$\dot U = (1/m_{A/C})(-D\cos\alpha + L\sin\alpha + F) + g\sin\theta - W\dot\theta \tag{2}$$

$$\dot W = (1/m_{A/C})(-L\cos\alpha - D\sin\alpha) + g\cos\theta + U\dot\theta \tag{3}$$

$$\ddot\theta = M/I_{yy} \tag{4}$$

The forces and moment were computed based on the aircraft state using the stability derivative method [10]. Each term can be calculated by using the appropriate coefficients according to the following example equation, where S is the aircraft wing area and $\bar c$ is the mean aerodynamic cord. The equation is easily repeated for drag and moment:

$$L = \tfrac{1}{2}\rho V^2 S(C_{L_0} + C_{L_\alpha}\alpha + C_{L_{\delta_e}}\delta_e + (\bar c/2U)(C_{L_{\dot\alpha}}\dot\alpha + C_{L_{\dot\theta}}\dot\theta)) \tag{5}$$

The stability derivatives were determined with a vortex-lattice method code based on the geometry of the Egrett and are shown in Table 1.

Wind disturbances are typically specified in an inertial frame with the vertical axis's positive direction pointing up. A new coordinate system, x, z, is defined in this way. The instantaneous wind can be

[§]Data on the U-2S/TU-2S is available online at http://www.af.mil/factsheets/factsheet.asp?fsID=129 [retrieved 1 July 2008].

[¶]Data available online at the Flinders University web site, http://ara.es.flinders.edu.au [retrieved 1 July 2008].

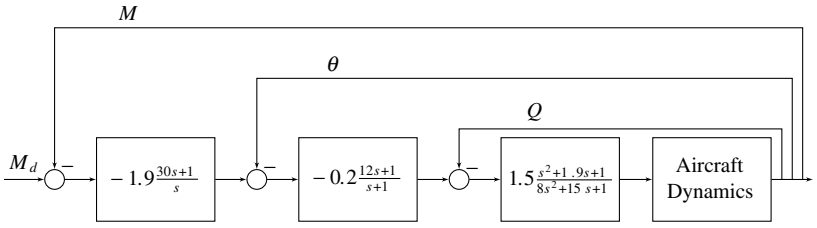

Fig. 1 Simulator autopilot block diagram for Mach hold with multiple loop closures.

supplied as a function of x, z, and possibly time. The wind speed was specified by an average nominal freestream velocity (subscript f) plus a disturbance quantity (subscript w). The true airspeeds U_a and W_a were computed at any time as the wind velocity $[U_f + U_w \quad W_w]^T$ minus the airframe speed relative to the ground $[U \quad W]^T$, with appropriate coordinate transformations:

$$\begin{bmatrix} U_a \\ W_a \end{bmatrix} = \mathbf{C}^T \left(\mathbf{C} \begin{bmatrix} U \\ W \end{bmatrix} - \begin{bmatrix} U_f + U_w \\ -W_w \end{bmatrix} \right) \tag{6}$$

The aircraft's inertial positions can be found by integrating the inertial velocities:

$$\begin{bmatrix} \dot{X} \\ \dot{Z} \end{bmatrix} = \mathbf{C} \begin{bmatrix} U \\ W \end{bmatrix} \tag{7}$$

The simulation was implemented in the MATLAB® Simulink environment. A fourth-order Runge–Kutta method was used to dynamically integrate the equations of motion during simulation runs.

The atmosphere was modeled using the 1976 U.S. Standard Atmosphere model. Various inputs were used for the turbulence model, which either introduced it as a perturbation to the atmospheric model or as a replacement for it.

To emulate typical high-altitude aircraft autopilots, an aggressive Mach hold controller was designed using classical control design techniques [11]. An elevator control signal was generated based on the error between the desired and actual Mach number, with dives to increase Mach and climbs to decrease it. The design goals for the autopilot were no steady-state error and a fast response time. A multiple loop closure technique was used, which allows the inner loops to be closed with good response times, the benefits of which are carried to the outer loops. The controller architecture is shown in Fig. 1.

Bode plots for the open-loop aircraft dynamics and closed-loop aircraft system with autopilot are shown in Fig. 2. Of note is that the controller eliminated steady-state error, illustrated by the plot going to 0 dB at low frequencies. Also, the bandwidth has been increased by a factor of 4, which suggests a faster system response. The frequencies of the two closed-loop system modes are 0.6 and 4.4 rad/s, which at the aircraft's cruise speed corresponds to wavelengths of 3400 and 450 ft.

Traditional Gust Sensitivity

The first simulation trial was conducted using traditional gust theory as an input. This theory states that a vertical gust with a $(1 - \cos)$ shape will disturb an aircraft by causing the wings to generate excess lift and increase the load factor. A discussion of the theory is provided by Raymer [9]. The equation

$$\Delta n = K \frac{\Delta L}{w} = K \frac{\rho W_w V S C_{L_\alpha}}{2 g m_{A/C}} \tag{8}$$

describes the extra load factor expected when encountering a vertical gust with magnitude W_w. The term K is a gust alleviation factor that accounts for the gust shape. Using the Egrett cruise conditions as parameters, the equation shows that a 15 ft/s vertical gust should result in a temporary increase to the load factor by 0.4. The results of a simulation using this gust as an input agree very well with the gust theory estimate, as shown in Fig. 3. Although the load factor plot

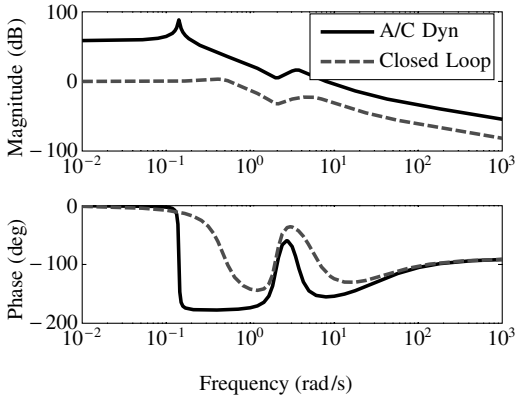

Fig. 2 Bode plots of open-loop aircraft dynamics with no controller and closed-loop system with autopilot.

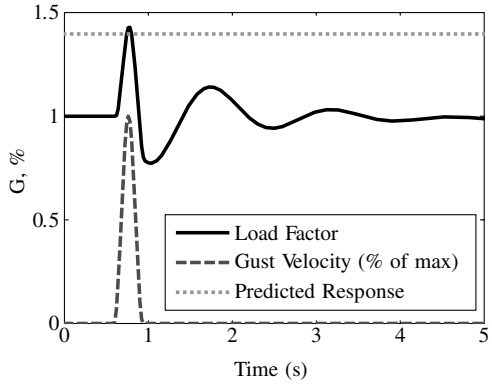

Fig. 3 Simulation response to a 15 ft/s (1 − cos) shaped vertical gust from gust sensitivity theory.

provides some confidence in the simulation, a single gust is not representative of the HAT problems reported by pilots.

Simple Gravity Wave Theory

A step closer to HAT realism is obtained with a simple model for flow over a mountain ridge. First, recall the wind coordinate system with x forward and z up, as is typical with atmospheric models. These models are often expressed using potential temperature, Θ, a result of the adiabatic relationships and defined [12] as follows:

$$\Theta(z) = T(z)[P_s / P(z)]^{(\gamma-1)/\gamma} \tag{9}$$

where P_s is usually taken as 100 kPa, close to sea level pressure. If a parcel of air expands or is compressed adiabatically, Θ remains constant, and so the Θ of a parcel of air is the temperature it would achieve if adiabatically compressed (or expanded) to 100 kPa. The gradient of Θ is a measure of the vertical stability of the atmosphere. If the gradient is positive and a parcel of air is lifted, it cools to a lower temperature than the surrounding atmosphere, and then it will decelerate and eventually sink toward its original location, generally

overshooting it and initiating an oscillation. A related quantity is the Brunt–Väisälä frequency, N, which is the natural frequency of a parcel of air with vertical motion only in a stable atmosphere, defined as

$$N^2 = \frac{g}{\Theta_f}\frac{d\Theta_f}{dz} \tag{10}$$

The simplest analytical equation for mountain wave motion is Long's equation for flow over a two-dimensional ridge [13]. Long's equation describes mountain waves that are stationary relative to the ground (not time varying). The formula is

$$(\partial^2\delta/\partial x^2) + (\partial^2\delta/\partial z^2) + (N^2/U_f^2)\delta = 0 \tag{11}$$

where δ is the vertical displacement of a streamline from its undisturbed height. The displacements will cause perturbations to the local values of horizontal and vertical velocities, U and W, and N. The simplest solution is

$$\delta(x, z) = A\sin(kx + mz) \tag{12}$$

such that

$$m^2 = N^2/U_f^2 - k^2 \tag{13}$$

where k is the horizontal wavelength, m is the vertical wavelength, and A is the amplitude. The horizontal wind velocity, the sum of the background and the wave perturbation, is then

$$U_w = U_f(1 - \partial\delta/\partial z) \qquad U_w = U_f(1 - Am\cos(kx + mz)) \tag{14}$$

The background vertical velocity of the wind is assumed to be zero, and so the vertical velocity is

$$W_w = U_f(\partial\delta/\partial x) \qquad W_w = U_f Ak\cos(kx + mz) \tag{15}$$

Θ is constant along the distorted streamlines. Using the isentropic relationship, a solution can be found for $\phi = \ell_n\,\Theta$.

$$\phi = \phi_o + B(z - A\sin(kx + mz)) \tag{16}$$

describes the effect of the linear wave field, where B is the background stability equal to $\mathrm{d}\phi/\mathrm{d}z$ and ϕ_o is the constant reference value (at $z = 0$).

The result of implementing Eqs. (14–16) is a wave with horizontal and vertical wind disturbances that are 180 deg out of phase and a temperature disturbance 90 deg out of phase with the wind disturbances. Temperature is determined by first computing the local ϕ and then using Eq. (9). These phase relationships are often observed by radiosondes ascending through a wave field [14].

As the wave changes the temperature, new fluid properties must be determined. A convenient analytical result can be found using the Boussinesq approximation, which is consistent with the mountain waves we are studying. With this assumption and assuming small perturbations, it can be shown [15] that

$$\rho' \approx -\rho_0(\Theta'/\Theta_f) \tag{17}$$

where the subscript 0 denotes the constant background density of the Boussinesq assumption, the prime is the perturbation caused by the gravity wave, and Θ_f is the undisturbed background for the altitude of observation before the disturbance. With this result, a perturbation pressure can also be determined, but it is second order compared with the density and temperature perturbations and can be ignored.

A range of discrete wavelengths of this disturbance type were used in the simulation. The vertical gust wave magnitude was kept at 15 ft/s by using a $\pm$7.5 ft/s wave. Fluctuations in horizontal velocity directly affect the Mach number and, because of the aggressive autopilot, have a greater effect on the load factor. Through trial runs of the simulation using single gusts, it was determined that a $\pm$2.5 ft/s horizontal wind gust produced an equivalent load factor disturbance as the $\pm$7.5 ft/s vertical wind speed wave. Similarly, at the Egrett's cruise altitude, a fluctuation in temperature of $\pm$8°R produces the same disturbance.

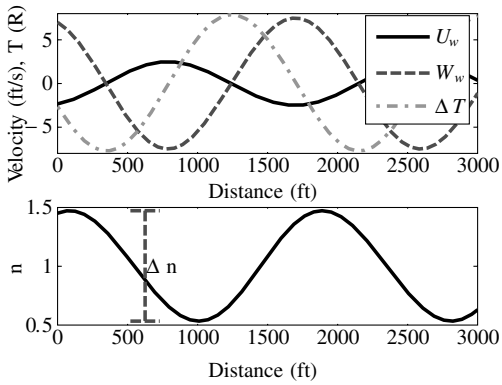

Fig. 4 Steady-state input and response of simulation to theoretical gravity wave, showing vertical and horizontal wind speeds and temperature out of phase.

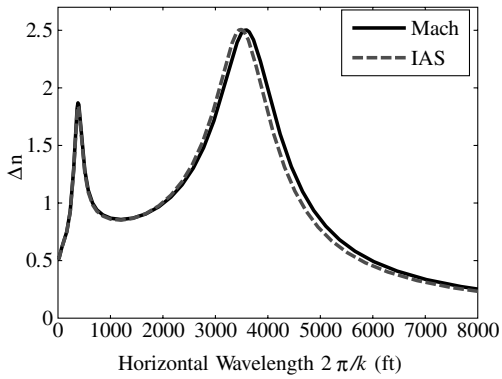

Fig. 5 Steady-state simulation response to analytical flow over a ridge at a range of wavelengths for both a Mach-following and indicated airspeed-following autopilot; the two peaks correspond to the aircraft's system modes.

For each wavelength considered, a steady-state condition was achieved after sufficient simulation time, and the difference between the maximum and minimum load factors was recorded. An example simulation trial is shown in Fig. 4. Notice the phasing of the components of the gravity wave input in the top plot. The bottom plot shows the calculated load factor output of the simulation at steady state.

The results for the entire sweep are plotted with the solid line in Fig. 5. The distinguishing feature of the plot is the presence of two dominant peaks. These peaks fall very close to the Egrett system modes. A separate simulation with isolated disturbances in horizontal and vertical gusts and temperature excursions revealed the nature of the peaks. The first, short wavelength peak was present in all cases, implying it was caused by a resonance associated with the aircraft dynamics. The second, longer wavelength peak was not present for the wave of vertical gusts, suggesting that an autopilot mode regulated changes in the Mach number. The wavelength of this second peak is close to the reported pilot accounts of low-frequency high-altitude turbulence, or Mach surf.

Atmospheric Simulation

Although the simple wave model was useful for determining the impact of the individual and ensemble property changes associated with a gravity wave, it is difficult to find a single monochromatic wave in the atmosphere [16]. For a more realistic atmospheric condition, the final disturbance type considered was a numerical simulation of flow over a ridge. A hybrid mesoscale and large eddy scale simulation with dynamic adaptive grid spacing was developed

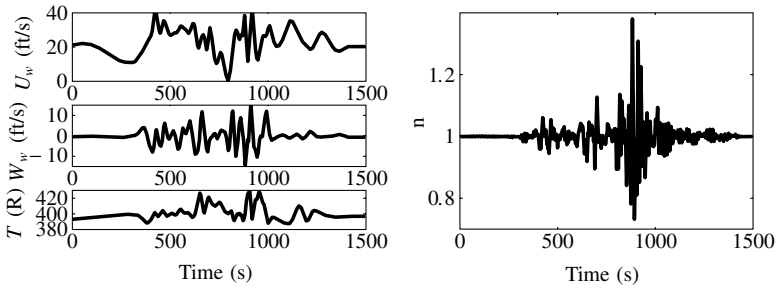

a) Input b) Output

Fig. 6 Simulation of data taken from the North Carolina State University hybrid mesoscale and large eddy scale simulation of flow over a ridge.

by North Carolina State University [17], and a trace of data from the results shown in Fig. 6a was used in the aircraft simulation. This case was a two-dimensional calculation with atmospheric properties extracted at 65 kft. Notice the large changes, especially in temperature, as the aircraft crosses the ridge at about 800 s and turbulence is encountered. The load factor output is shown in Fig. 6b.

Autopilot Temperature Sensitivity

Through simulation, the U-2 and the Egrett were shown to be sensitive to high-altitude turbulence due to the strong reaction of the autopilot to temperature changes and horizontal gusts. A logical mitigation effort would be to design an autopilot less sensitive to temperature disturbances. It has been suggested that a possible strategy is to use an autopilot tracking indicated airspeed instead of the strategy used by U-2 aircraft, which tracks Mach number. To determine the validity of this suggestion, a sensitivity analysis was performed. For the purposes of this comparison, the term sensitivity refers to the relative change of the sensed variable used as the input to the autopilot given a change in atmospheric temperature.

McCormick [18] has a good treatment of traditional speed sensing theory. The Mach number is the ratio of aircraft speed to the speed of sound, a:

$$M = V/a = V/\sqrt{\gamma RT} \tag{18}$$

where a was expanded using the equation of state with the specific heat ratio for air γ and the specific gas constant for air R. Manipulating the compressible Bernoulli equation yields a solution for the calibrated airspeed, which is equivalent to the indicated airspeed (IAS) if a perfectly calibrated instrument is assumed:

$$V_{\mathrm{IAS}} = \sqrt{\frac{2a_{\mathrm{sl}}^2}{\gamma - 1}\left[\left(\frac{\Delta p}{p_{\mathrm{sl}}} + 1\right)^{\frac{\gamma-1}{\gamma}} - 1\right]} \tag{19}$$

where Δp is the difference between the pressures as sensed by the total and static pressure taps, and the subscript sl refers to sea level conditions.

A constant Mach number autopilot would compute the actual Mach number using the familiar equation

$$M = \sqrt{\frac{2}{\gamma - 1}\left[\left(\frac{p_0}{p}\right)^{\frac{\gamma-1}{\gamma}} - 1\right]} \tag{20}$$

where p_0 is the total pressure measured at the stagnation point of the pitot-static probe. In effect, the Mach number hold tries to maintain a constant ratio of the static and total pressure, and the indicated air speed hold tries to maintain a constant difference between the two pressures.

The relative sensitivity can be found by taking a partial derivative with respect to a variable and dividing by the original quantity. The relative sensitivity of Mach, Eq. (18), to temperature is

$$S_T^M = (1/M)(\partial M/\partial T) = -(1/2T) \tag{21}$$

The derivative for the IAS, Eq. (19), is more complicated, but after simplification the relative sensitivity becomes

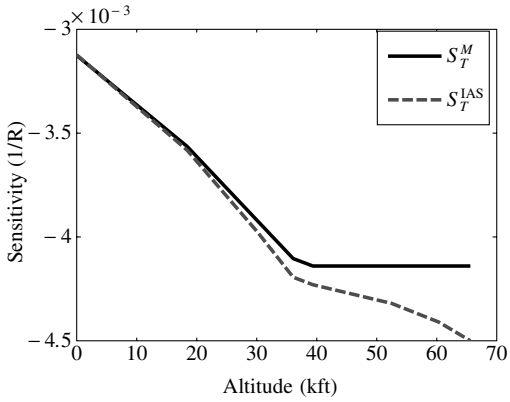

Fig. 7 Effect of altitude on the sensitivity of Mach and IAS to temperature; the curves diverge after the tropopause and when compressibility effects become significant.

$$S_T^{\mathrm{IAS}} = -\frac{1}{2T}\frac{a_{\mathrm{sl}}^2 M^2 p}{p_{\mathrm{sl}} V_{\mathrm{IAS}}^2}\left(\frac{p_{\mathrm{sl}} p_0}{p(p_{\mathrm{sl}} + \Delta p)}\right)^{\frac{1}{\gamma}} \tag{22}$$

where Eq. (20) was used to compute p_0.

The indicated airspeed sensitivity has the same $-(1/2T)$ term as the Mach sensitivity, along with other terms that involve altitude and compressibility effects. A profile of the two sensitivities over a range of altitudes for an aircraft flying at a constant indicated airspeed of 165 ft/s, which is the Egrett cruise condition, is shown in Fig. 7. The two curves diverge rapidly after the tropopause at about 36 kft, at which point the aircraft's Mach number is 0.3. Above the tropopause, the atmospheric model maintained an approximately constant air temperature, holding the Mach sensitivity steady. In addition, true airspeed increases at altitudes higher than this, and compressibility becomes even more of a factor. Note that the figure was constructed using two independent methods: the sensitivity equations (21) and (22) and a finite difference approach to the equation for the Mach number (18) and indicated airspeed (19); the computed curves were nearly identical.

The plot implies that autopilots tracking indicated airspeed will be just as or slightly more susceptible to HAT encounters. To verify these results, the Egrett simulation's autopilot was modified to track IAS instead of Mach number, after an appropriate gain change in the outer loop. The results were nearly identical, as shown by the dashed line in Fig. 5. This is expected due to the similar sensitivities of the two variables at the Egrett cruise altitude.

Effect of Temperature on Flight Envelope

The temperature disturbances inherent in HAT also disturb the flight envelope. An aircraft is bound in terms of the altitude and speeds at which it can fly. If the speed is too slow, the lift necessary to overcome the aircraft weight requires a coefficient of lift larger than the aircraft's maximum; this is a stall condition. On the other hand, if the speed is too great, the Mach number exceeds the aircraft's critical

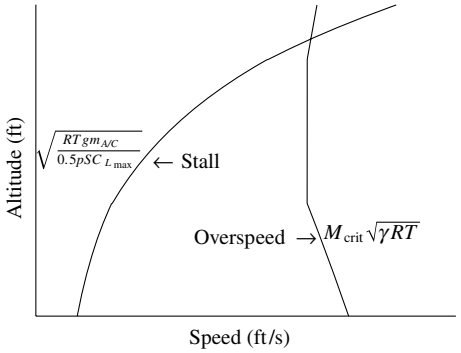

Fig. 8 Diagram of flight envelope bounded by stall and critical Mach number.

Mach number. This overspeeding creates a local supersonic flow that can cause a Mach buffet and structural failure. These bounds are known as the flight envelope. High-altitude reconnaissance aircraft such as the U-2 fly near the top of the envelope, without much room for fluctuations in airspeed; however, changing atmospheric density and temperature causes the envelope to change. There is a dangerous possibility of a stall leading to overspeeding if the pilot overcompensates.

During a HAT encounter, temperature fluctuations cause both limits of the envelope to move. As is shown in Fig. 8, the stall line is governed by the equation

$$V_{\text{stall}} = \sqrt{\frac{gm_{A/C}}{0.5\rho SC_{L_{\max}}}} = \sqrt{\frac{gm_{A/C}RT}{0.5pSC_{L_{\max}}}} \tag{23}$$

and the overspeed line is governed by the equation

$$V_{\text{crit}} = M_{\text{crit}}\sqrt{\gamma RT} \tag{24}$$

where M_{crit} is the Mach number at which the local flow around the airframe becomes supersonic. Thus, if the temperature decreases during a turbulent encounter it will cause the stall speed to decrease. Also, the critical Mach buffet speed will be lowered. This shifting of the flyable region with temperature can cause potentially dangerous environments with aircraft flying in the narrow band near the top of their envelope. It is fortuitous that the temperature decrease will also result in the autopilot attempting to decrease the aircraft speed, effectively trying to keep it in the envelope. Unfortunately, response times can be slower than the frequency of atmospheric changes, resulting in possible out-of-phase behavior.

Flight Data

The best information about HAT comes from flight data, and a relationship with Flinders University in Adelaide, Australia, provides the opportunity to collect this data through their Egrett research flights. Because these aircraft are equipped with a suite of high-precision sensors, including the "best" aircraft turbulence (BAT) probe [19] and a high data acquisition rate to characterize the environment, they are well suited for the task. Jet stream induced wave turbulence is frequently encountered in their operating area because the stream shifts in and out of the region. A data set from one of the Egrett missions, documented by Wroblewski et al. [20], was used to generate a PSD of the horizontal wind velocity as measured by the BAT probe on the aircraft. In Fig. 9, the PSD from the flight data is compared with the aforementioned military and federal aviation standards.

Notice the large peak in the curve at about 0.01 Hz. At the flight cruise condition, this is equivalent to a wavelength of about 1 mile, which matches well within what was reported by U-2 pilots. An additional feature of the PSD comparison is that the observed fluctuating wind speed power is greater than either of the specifications at this frequency.

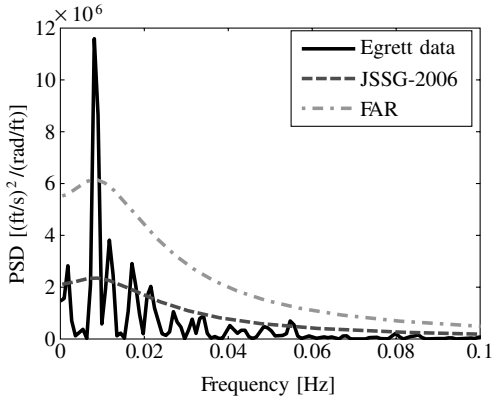

Fig. 9 PSD of horizontal wind velocity sensed by Egrett compared with design standards; the standards are exceeded at a frequency consistent with pilot accounts of in-flight turbulence.

Conclusions

High-altitude turbulence has a pervasive impact on U-2 missions, and its effect on UAVs has not been thoroughly studied. Simulation has confirmed that major factors driving the flight disturbances are temperature excursions and horizontal wind speed changes induced by gravity waves breaking into turbulence, and the autopilot's aggressive response. A sensitivity analysis has shown that using an autopilot based on indicated airspeed will not alleviate the issue. Studying the flight envelope showed that temperature changes shift the envelope of viable airspeeds, exacerbating the problem.

Current regulations contain no turbulence requirements based on temperature disturbances. Additionally, flight data analysis shows that specified classifications of horizontal wind turbulence at high altitudes may be deficient. It is recommended that these regulations be reassessed in light of new findings in HAT research, and that current and future unmanned high-altitude aircraft consider the high-altitude turbulence environment when designing and testing their autonomous control algorithms.

Acknowledgments

The authors gratefully acknowledge the support they received on this project. Steve Brandt and Ray Whitford, Department of Aeronautics, Air Force Academy, were very helpful in getting our simulation effort off the ground with their week-long fighter aircraft design course. Michael Walker with Andrew Kopeikin started this effort and laid a great foundation for the rest of the program. Robert Ficarra of the Lockheed Martin Aeronautics Company was instrumental in the delivery of the U-2 simulation parameters. James Scoville of the Air Force Research Laboratory did some great work with our sensitivity analysis. We thank the program manager for the basic research portion of this program, Arje Nachman, Air Force Office of Scientific Research. We thank Owen Cote of our laboratory, Jorg Hacker of Airborn Research Australia, Flinders University, and Don Wroblewski of Boston University for helping with the Egrett information and data. We thank Scott McRae, Hassan Hassan, and Xudong Xiao of North Carolina State University. We also thank our section chiefs during this effort, Donald Norquist and Frank Ruggiero, and our branch chief, Robert Beland, for their encouragement and support.

References

[1] Ehernberger, L. J., "Stratospheric Turbulence Measurements and Models for Aerospace Plane Design," AIAA Paper 92-5072, Dec. 1992.

[2] Fritts, D. C., and Alexander, M. J., "Gravity Wave Dynamics and Effects in the Middle Atmosphere," *Reviews of Geophysics*, Vol. 41, No. 1, 2003, pp. 3-1–3-64. doi:10.1029/2001RG000106

[3] Werne, J., and Fritts, D. C., "Stratified Shear Turbulence: Evolution and Statistics," *Geophysical Research Letters*, Vol. 26, No. 4, 1999, pp. 439–442.

doi:10.1029/1999GL900022
[4] "Code of Federal Regulations", Federal Aviation Administration, Title 14, Part 25, Appendix G, 2005.
[5] "Aircraft Structures", Dept. of Defense JSSG-2006, 1998.
[6] Crawford, T. L., and Dobosy, R. J., "A Sensitive Fast-Response Probe to Measure Turbulence and Heat Flux from Any Airplane," *Boundary Layer Meteorology*, Vol. 59, No. 3, May 1992, pp. 257–278. doi:10.1007/BF00119816
[7] Torgerson, J., Walker, M., Kopeikin, A., and Jumper, G., "Modeling Flight Through Clear Air Turbulence," AIAA Paper 2006-73, 2006.
[8] Stevens, B. L., and Lewis, F. L., *Aircraft Control and Simulation*, 2nd ed., Wiley, New York, 2003.
[9] Raymer, D. P., *Aircraft Design: A Conceptual Approach*, 3rd ed., AIAA Education Series, AIAA, Reston, VA, 1999.
[10] Etkin, B., and Reid, L. D., *Dynamics of Flight, Stability and Control*, 3rd ed., Wiley, New York, 1996.
[11] Nelson, R. C., *Flight Stability and Automatic Control*, McGraw–Hill, New York, 1998.
[12] Hess, S. L., *Introduction to Theoretical Meteorology*, Holt, Rinehart and Winston, New York, 1958.
[13] Scorer, R. S., "Theory of Airflow over Mountains 2: The Flow over a Ridge," *Quarterly Journal of the Royal Meteorological Society*, Vol. 79, No. 339, 1953, pp. 70–83. doi:10.1002/qj.49707933906
[14] Shutts, G. J., Kitchen, M., and Hoare, P. H., "A Large Amplitude Gravity Wave in the Lower Stratosphere Detected by Radiosonde," *Quarterly Journal of the Royal Meteorological Society*, Vol. 114, No. 481, 1988, pp. 579–594. doi:10.1256/smsqj.48102
[15] Holton, J. R., *An Introduction to Dynamic Meteorology*, Vol. 48, 3rd ed., International Geophysics Series, Academic Press, San Diego, CA, 1992.
[16] Jumper, G. Y., Murphy, E. A., Ruggiero, F. H., Ratkowski, J. R., Vernin, J., and Trinquet, H., "OHP-APT 2002 Gravity Wave Campaign: Waves, Turbulence and Forecasts," *Environmental Fluid Mechanics*, Vol. 7, No. 5, 2007, pp. 351–370. doi:10.1007/s10652-007-9030-y
[17] Xiao, X., McRae, D. S., and Hassan, H. A., "Dynamically Resolved Simulation of Atmospheric Features and Turbulence—Initial Results," AIAAPaper 2005-0265, 2005.
[18] McCormick, B. W., *Aerodynamics, Aeronautics, and Flight Mechanics*, 2nd ed., Wiley, New York, 1995.
[19] Hacker, J. M., and Crawford, T. L., "The BAT-Probe: The Ultimate Probe to Measure Turbulence from Any Kind of Aircraft (or Sailplane)," *Technical Soaring*, Vol. 23, No. 2, 1999, pp. 43–46.
[20] Wroblewski, D. E., Cote, O. R., Hacker, J. M., and Dobosy, R. J., "Cliff-Ramp Patterns and Kelvin-Helmholtz Billows in Stably Stratified Shear Flow in the Upper Troposphere: Analysis of Aircraft Measurements," *Journal of the Atmospheric Sciences*, Vol. 64, No. 7, July 2007, pp. 2521–2539. doi:10.1175/JAS3956.1